J|A|C|S
ARTICLES
Published on Web 07/29/2006

A Porous Framework Polymer Based on a Zinc(II) 4,4′-Bipyridine-2,6,2′,6′-tetracarboxylate: Synthesis, Structure, and "Zeolite-Like" Behaviors

Xiang Lin, Alexander J. Blake, Claire Wilson, Xue Zhong Sun, Neil R. Champness,* Michael W. George, Peter Hubberstey,* Robert Mokaya, and Martin Schröder*

Contribution from the School of Chemistry, The University of Nottingham, University Park, Nottingham, NG7 2RD, United Kingdom

Received February 8, 2006; E-mail: m.schroder@nottingham.ac.uk

Abstract: The robust metal−organic framework compound $\{[Zn_2(L)]\cdot 4H_2O\}_\infty$ **I** has been synthesized by hydrothermal reaction of $ZnCl_2$ and 4,4′-bipyridine-2,6,2′,6′-tetracarboxylic acid (H_4L). Compound **I** crystallizes in a chiral space group, $P4_22_12$, with the chirality generated by the helical chains of hydrogen-bonded guest water molecules rather than by the coordination framework. Removal of guest water molecules from the crystal affords the porous material, $[Zn_2(L)]_\infty$ (**II**), which has very high thermal stability and is chemically inert. The N_2 isotherm of **II** at 77 K suggests a uniform porous structure with a BET surface area of 312.7 m^2/g and a remarkably strong interaction with N_2 molecules ($\beta E_0 = 29.6$ kJ mol^{-1}). **II** also exhibits significant gas storage capacities of 1.08 wt % for H_2 at 4 bar and 77 K and 3.14 wt % (44.0 cm^3/g, 67 v/v) for methane at 9 Bar at 298 K. The adsorption behavior of **II** toward organic solvent vapors has also been studied, and isotherms reveal that for different solvent vapors adsorption is dominated by two types of processes, absorbate−absorbate or absorbate−absorbent interactions. The adsorption and desorption kinetic processes in **II** are determined mainly by the molecular size of the guest species and their interaction with the host.

Introduction

The design and synthesis of porous materials based on the coordinative bonding between metal ions and organic linker ligands has proven to be a flexible and versatile approach to new functional materals.[1−4] Those materials with accessible voids may be considered to be metal−organic analogues of porous zeolites and are of interest as new materials with applications for gas storage (e.g., of hydrogen or methane), small molecule separation, and enantiomer resolution.[2,3,5] Although there are now a vast number of coordination polymers reported, few are able to take up and release guest molecules in a reversible manner. These include the series of compounds based upon di- or tri-topic benzoic acids,[3,4,6−8] and framework compounds based on Cu^{II}, 4,4′-bipyridine, and octahedral anions (SiF_6^{2-}, GeF_6^{2-}, and PF_6^-).[9] Chiral ligands derived from tartaric acid have been used to prepare a homochiral framework compound which is enantioselective for small molecules,[10] while chiral topologies can also be generated from nonchiral components by using an auxiliary ligand in the synthesis of a metal−organic framework compound.[11,12]

Recent studies have shown the great potential of coordination framework compounds for gas storage, particularly for hydrogen[13−17] and methane.[8,18,19] Analogous to the hydrogen adsorp-

(1) (a) Oh, M.; Carpenter, G. B.; Sweigart, D. A. *Acc. Chem. Res.* **2004**, *37*, 1−11. (b) Ockwig, N. W.; Delgado-Friedrichs, O.; O'Keeffe, M.; Yaghi, O. M. *Acc. Chem. Res.* **2005**, *38*, 176−182. (c) Cotton, F. A.; Lin, C.; Murillo, C. A. *Acc. Chem. Res.* **2001**, *34*, 759−771. (d) Rowsell, J. L. C.; Yaghi, O. M. *Angew. Chem., Int. Ed.* **2005**, *44*, 4670−4679. (e) Sudik, A. C.; Millward, A. R.; Ockwig, N. W.; Cote, A. P.; Kim, J.; Yaghi, O. M. *J. Am. Chem. Soc.* **2005**, *127*, 7110−7118.

(2) (a) Ferey, G.; Mellot-Draznieks, C.; Serre, C.; Millange, F. *Acc. Chem. Res.* **2005**, *38*, 217−225. (b) Bradshaw, D.; Claridge, J. B.; Cussen, E. J.; Prior, T. J.; Rosseinsky, M. J. *Acc. Chem. Res.* **2005**, *38*, 273−282. (c) Matsuda, R.; Kitaura, R.; Kitagawa, S.; Kubota, Y.; Belosludov, R. V.; Kobayashi, T. C.; Sakamoto, H.; Chiba, T.; Takata, M.; Kawazoe, Y.; Mita, Y. *Nature* **2005**, *436*, 238−241.

(3) Yaghi, O. M.; O'Keeffe, M.; Ockwig, N. W.; Chae, H. K.; Eddaoudi, M.; Kim, J. *Nature* **2003**, *423*, 705−714.

(4) Rosi, N. L.; Kim, J.; Eddaoudi, M.; Chen, B. L.; O'Keeffe, M.; Yaghi, O. M. *J. Am. Chem. Soc.* **2005**, *127*, 1504−1518.

(5) (a) Rosseinsky, M. J. *Microporous Mesoporous Mater.* **2004**, *73*, 15−30. (b) Matsuda, R.; Kitaura, R.; Kitagawa, S.; Kubota, Y.; Belosludov Rodion, V.; Kobayashi Tatsuo, C.; Sakamoto, H.; Chiba, T.; Takata, M.; Kawazoe, Y.; Mita, Y. *Nature* **2005**, *436*, 238−241. (c) Ferey, G.; Mellot-Draznieks, C.; Serre, C.; Millange, F.; Dutour, J.; Surble, S.; Margiolaki, I. *Science* **2005**, *309*, 2040−2042. (d) Kitaura, R.; Kitagawa, S.; Kubota, Y.; Kobayashi Tatsuo, C.; Kindo, K.; Mita, Y.; Matsuo, A.; Kobayashi, M.; Chang, H.-C.; Ozawa Tadashi, C.; Suzuki, M.; Sakata, M.; Takata, M. *Science* **2002**, *298*, 2358−2361.

(6) (a) Eddaoudi, M.; Moler, D. B.; Li, H. L.; Chen, B. L.; Reineke, T. M.; O'Keeffe, M.; Yaghi, O. M. *Acc. Chem. Res.* **2001**, *34*, 319−330. (b) Eddaoudi, M.; Li, H. L.; Yaghi, O. M. *J. Am. Chem. Soc.* **2000**, *122*, 1391−1397. (c) Rowsell, J. L. C.; Yaghi, O. M. *Microporous Mesoporous Mater.* **2004**, *73*, 3−14.

(7) Chae, H. K.; Siberio-Perez, D. Y.; Kim, J.; Go, Y.; Eddaoudi, M.; Matzger, A. J.; O'Keeffe, M.; Yaghi, O. M. *Nature* **2004**, *427*, 523−527.

(8) Eddaoudi, M.; Kim, J.; Rosi, N.; Vodak, D.; Wachter, J.; O'Keefe, M.; Yaghi, O. M. *Science* **2002**, *295*, 469−472.

(9) Noro, S.; Kitaura, R.; Kondo, M.; Kitagawa, S.; Ishii, T.; Matsuzaka, H.; Yamashita, M. *J. Am. Chem. Soc.* **2002**, *124*, 2568−2583.

(10) Seo, J. S.; Whang, D.; Lee, H.; Jun, S. I.; Oh, J.; Jeon, Y. J.; Kim, K. *Nature* **2000**, *404*, 982−986.

(11) Kepert, C. J.; Prior, T. J.; Rosseinsky, M. J. *J. Am. Chem. Soc.* **2000**, *122*, 5158−5168.

(12) Bradshaw, D.; Prior, T. J.; Cussen, E. J.; Claridge, J. B.; Rosseinsky, M. J. *J. Am. Chem. Soc.* **2004**, *126*, 6106−6114.

(13) Rowsell, J. L. C.; Millward, A. R.; Park, K. S.; Yaghi, O. M. *J. Am. Chem. Soc.* **2004**, *126*, 5666−5667.

(14) (a) Kaye, S. S.; Long, J. R. *J. Am. Chem. Soc.* **2005**, *127*, 6506−6507. (b) Rowsell, J. L. C.; Eckert, J.; Yaghi, O. M. *J. Am. Chem. Soc.* **2005**, *127*, 14904−14910.

tion on carbon materials[20] and zeolites,[21] coordination frameworks use their microporous structure to restrain hydrogen molecules. The advantage of such framework materials lies in the possibility of producing porous materials in a crystalline form endowed with a uniform porous structure and good phase purity. In addition, varying the linking ligand within these structures offers opportunities and flexibility to modify and tune the porous structure, thus resulting in different adsorption properties tailored for specific absorbates. Reversible physisorption of H_2 has been reported[13−17] for a series of coordination framework compounds having a range of structures and pore sizes. Hysteretic H_2 adsorption−desorption has also been observed in $Ni_2(bipy)_3(NO_3)_4$, showing that hydrogen may be "kinetically trapped" in the porous structure at 77 K and released gradually above 110 K. This kinetic trapping effect is related to the flexibility of the porous framework materials.[15]

Preparing open and robust frameworks based on metal-organic nodes and linkers remains a major challenge since most coordination frameworks undergo structural change or collapse upon removal of their guest molecules. Change of coordination geometry at the metal site during desolvation is the most common cause of the instability of the framework. Some recent studies have indicated possible strategies[22] to avoid this by preventing the initial coordination of solvent molecules to the metal atom. In a series of metal−organic framework compounds, the $[Zn_4O]$ node is coordinated only by carboxylate groups[3,7,8] to form frameworks that are very stable to the removal of guest molecules from the pores. However, the $[Zn_4O]$ node is sensitive to water, and exposure to moisture or acid results in the collapse of the framework structure.[23,24] A stable framework compound

Scheme 1. H_4L

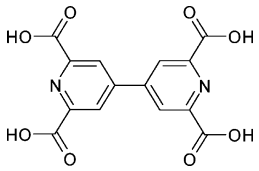

prepared from 2,2′-bipyridyl-5,5′-dicarboxylic acid with $MnCl_2$ in which the donor atoms on the ligand occupy all the coordination sites of Mn(II) has been reported,[25] while a diamine ligand has been used to bind to the axial sites of a $Zn_2(carboxylate)_4$ paddlewheel to afford a more robust framework.[17] Our own recent work has focused on the design and synthesis of a wide range of new d- and f-block metal−organic framework materials showing unusual and unique topologies and structure.[26] We report herein a novel framework material $[Zn(L)]_\infty$ based on Zn(II) bound to the tetraanion of 4,4′-bipyridine-2,6,2′,6′-tetracarboxylic acid (H_4L, see Scheme 1). The ligand has two carboxylate O and one N donor at each end, and this donor set forms a very stable tridentate binding synthon with metal ions, while the other O-donor of each carboxylate group can coordinate to other metal atoms in competition with solvent molecules. The resulting material has a highly stable framework structure and reversibly and selectively absorbs organic molecules, H_2, and methane into the framework pores.

Experimental Section

General. All reagents not specifically listed below were obtained from commercial sources and were used as received. 4,4′-Bipyridine-2,6,2′,6′-tetracarboxylic acid (H_4L) was prepared according to the literature procedure.[27] Anhydrous solvents were used in isotherm measurements: THF, diethyl ether, hexane, pentane, and toluene were dried by passage through a silica column, anhydrous chloroform was distilled over calcium hydride before use, and methanol was dried by distillation from Mg. IR spectra were recorded on KBr plates using a Nicolet Avatar 360 FT-IR spectrophotometer. The diffuse reflectance IR spectra (DRIFTS) were recorded on a Nicolet AVATAR-360 FT-IR spectrophotometer equipped with an MCT detector with a Spectra-Tech Collector 0030-0xx kit. X-ray powder diffractograms were recorded on a Philips X'pert powder diffractometer. Thermal gravimetric analyses were performed on a TA SDT-Q600.

Synthesis. A. $\{[Zn_2(L)]\cdot 4H_2O\}_\infty$ (I). In a typical run, H_4L (0.1660 g, 0.50 mmol), $ZnCl_2$ (0.137 g, 1.00 mmol), and 2,6-lutidine (0.22 g, 2.00 mmol) were mixed in water (30 mL) and sealed in a 45 mL Parr bomb. The bomb was heated in an oven at the rate of 1 °C/min up to 130 °C and kept at this temperature for 6 days. The oven was switched off, and the bomb was left to cool to room temperature. The colorless microcrystalline product was separated by filtration, washed sequentially with deionized water, EtOH, and Et_2O, and then dried in air. Yield

(15) Zhao, X. B.; Xiao, B.; Fletcher, A. J.; Thomas, K. M.; Bradshaw, D.; Rosseinsky, M. J. *Science* **2004**, *306*, 1012−1015.
(16) (a) Ferey, G.; Latroche, M.; Serre, C.; Millange, F.; Loiseau, T.; Percheron-Guegan, A. *Chem. Commun.* **2003**, 2976−2977. (b) Chen, B.; Ockwig, N. W.; Millward, A. R.; Contreras, D. S.; Yaghi, O. M. *Angew. Chem., Int. Ed.* **2005**, *44*, 2−5.
(17) Chun, H.; Dybtsev, D. N.; Kim, H.; Kim, K. *Chem.−Eur. J.* **2005**, *11*, 3521−3529.
(18) Duren, T.; Sarkisov, L.; Yaghi, O. M.; Snurr, R. Q. *Langmuir* **2004**, *20*, 2683−2689.
(19) Noro, S.; Kitagawa, S.; Kondo, M.; Seki, K. *Angew. Chem., Int. Ed.* **2000**, *39*, 2082−2084.
(20) (a) Ströbel, R.; Schliermann, L. J. T.; Trapp, V.; Schütz, W.; Bohmhammel, K.; Wolf, G.; Garche, J. *J. Power Sources* **1999**, *84*, 221−224. (b) Gundiah, G.; Govindaraj, A.; Rajalakshmi, N.; Dhathathreyan, K. S.; Rao, C. N. R. *J. Mater. Chem.* **2003**, *13*, 209−213. (c) Smith, M. R.; Bittner, E. W.; Shi, W.; Johnson, J. K.; Bockrath, B. C. *J. Phys. Chem. B* **2003**, *107*, 3752−3760.
(21) (a) Weitkamp, J.; Fritz, M.; Ernst, S. *Int. J. Hydrogen Energy* **1995**, *20*, 967−970. (b) van den Berg, A. W. C.; Bromley, S. T.; Flikkema, E.; Wojdel, J.; Maschmeyer, T.; Jansen, J. C. *J. Chem. Phys.* **2004**, *120*, 10285−10289. (c) Arean, C. O.; Manoilova, O. V.; Bonelli, B.; Delgado, M. R.; Palomino, G. T.; Garrone, E. *Chem. Phy. Lett.* **2003**, *370*, 631−635. (d) Forster, P. M.; Eckert, J.; Chang, J.-S.; Park, S.-E.; Ferey, G.; Cheetham, A. K. *J. Am. Chem. Soc.* **2003**, *125*, 1309−1312.
(22) For examples of evacuated pores in metal−organic framework materials see: (a) Arahams, B. F.; Jackson, P. A.; Robson, R. *Angew. Chem., Int. Ed.* **1998**, *37*, 2656−2659. (b) Reineke, T. M.; Eddaoudi, M.; Fehr, M.; Kelley, D.; Yaghi, O. M. *J. Am. Chem. Soc.* **1999**, *121*, 1651−1657. (c) Pan, L.; Huang, X.; Li, J.; Wu, Y.; Zheng, N. *Angew. Chem., Int. Ed.* **2000**, *39*, 527−530. (d) Cao, R.; Sun, D.; Liang, Y.; Hong, M.; Tatsumi, K.; Shi, Q. *Inorg. Chem.* **2002**, *41*, 2087−2094. (e) Biradha, K.; Fujita, M. *Angew. Chem., Int. Ed.* **2002**, *41*, 3392−3395. (f) Suh, M. P.; Ko, J. W.; Choi, H. J. *J. Am. Chem. Soc.* **2002**, *124*, 10976−10977. (g) Pan, L.; Adams, K. M.; Hernandez, H. E.; Wang, X.; Zheng, C.; Hattori, Y.; Kaneko, K. *J. Am. Chem. Soc.* **2003**, *125*, 3062−3067. (h) Hanson, K.; Calin, N.; Bugaris, D.; Scancela, M.; Sevov, S. C. *J. Am. Chem. Soc.* **2004**, *126*, 10502−10503. (i) Dinca, M.; Long, J. R. *J. Am. Chem. Soc.* **2005**, *127*, 9376−9377. (j) Takaoka, K.; Kawano, M.; Tominaga, M.; Fujita, M. *Angew. Chem., Int. Ed.* **2005**, *44*, 2151−2154. (k) Chen, C. L.; Goforth, A. M.; Smith, M. D.; Su, C.-Y.; zur Loye, H.-C. *Angew. Chem., Int. Ed.* **2005**, *44*, 6673−6677.
(23) Panella, B.; Hirscher, M. *Adv. Mater.* **2005**, *17*, 538−541.
(24) Huang, L. M.; Wang, H. T.; Chen, J. X.; Wang, Z. B.; Sun, J. Y.; Zhao, D. Y.; Yan, Y. S. *Microporous Mesoporous Mater.* **2003**, *58*, 105−114.
(25) Tynan, E.; Jensen, P.; Kruger, P. E.; Lees, A. C. *Chem. Commun.* **2004**, 776−777.
(26) (a) Blake, A. J.; Brooks, N. R.; Champness, N. R.; Hanton, L. R.; Hubberstey, P.; Schröder, M. *Pure and Applied Chemistry* **1998**, *70*, 2351−2357. (b) Blake, A. J.; Champness, N. R.; Khlobystov, A. N.; Parsons, S.; Schröder, M. *Angew. Chem., Int. Ed.* **2000**, *39*, 2317−2320. (c) Champness, N. R.; Schröder, M. *Current Opinion in Solid State and Materials Chemistry* **1998**, *3*, 419−424. (d) Withersby, M. A.; Blake, A. J.; Champness, N. R.; Cooke, P. A.; Hubberstey, P.; Realf, A. L.; Schröder, M. *J. Chem. Soc., Dalton Trans.* **2000**, 3261−3268. (e) Blake, A. J.; Brooks, N. R.; Champness, N. R.; Crew, M.; Deveson, A.; Fenske, D.; Gregory, D. H.; Hanton, L. R.; Hubberstey, P.; Schröder, M. *Chem. Commun.* **2001**, 1432−1433. (f) Long, D.-L.; Blake, A. J.; Champness, N. R.; Wilson, C.; Schröder, M. *Angew. Chem., Int. Ed.* **2001**, *40*, 2443−2447. (g) Long, D.-L.; Blake, A. J.; Champness, N. R.; Wilson, C.; Schröder, M. *Chem.−Eur. J.* **2002**, *8*, 2026−2033. (h) Williams, C. A.; Blake, A. J.; Hubberstey, P.; Schröder, M. *Chem. Commun.* **2005**, 5435−5437. (i) Hubberstey, P.; Schröder, M.; Champness, N. R. *J. Solid State Chem.* **2005**, *178*, 2414−2419.
(27) Huenig, S.; Wehner, I. *Synthesis* **1989**, 552−554.

0.2015 g (76%). Selected IR(KBr): ν = 1684(vs), 1649(vs), 1625(s), 1609(vs), 1564(m), 1456(s), 1382(vs), 1308(vs), 1182(s), 1077(s), 906-(m), 796(m), 750(s), 698(m), 677(m), 491(m) cm^{-1}. Anal. Calcd (Found) for $Zn_2C_{14}N_2O_{12}H_{12}$: C, 31.66 (32.74); H, 2.28 (2.16); N, 5.28 (5.46). This "as synthesized" sample of **I** can be readily transformed to the anhydrous form $[Zn_2(L)]_\infty$ (**II**) by heating to 100 °C in air. Satisfactory elemental analysis results were obtained from this anhydrous sample (**II**).

Crystals suitable for single-crystal X-ray diffraction structure analysis were obtained by the following procedure. H_4L (0.0332 g, 0.10 mmol), $ZnCl_2$ (0.0274 g, 0.2 mmol), and 1,3,5-tri(4-pyridyl)-benzene (0.041 g, 0.13 mmol) were mixed in water (8 mL) and sealed in a 45 mL Parr bomb. The bomb was slowly heated in an oven up to 130 °C at the rate of 0.1 °C/min and kept at this temperature for 6 days, before the oven was cooled to room temperature at the rate of 0.2 °C/min. The crystalline product was separated by filtration and washed with deionized water, EtOH, and Et_2O. In the best run, 0.0162 g (Yield: 31%) of colorless block-shaped crystals with the largest dimension up to 0.25 mm were obtained.

B. $[Zn_2(L)]_\infty$ (II). Compound **II** can be prepared from **I** by heating **I** to 100 °C for 1 h in an oven or by exposure of **I** under an anhydrous environment, e.g., dynamic vacuum or dried nitrogen flow at room temperature. Anal. Calcd (Found) for $Zn_2C_{14}N_2O_8H_4$: C, 36.64 (36.49); H, 0.88 (0.93); N, 6.01 (6.07).

C. $[Zn_2(L)]_\infty$·0.55Benzene (III). Compound **I** was dehydrated by heating to 100 °C for 1 h in an oven, and after removing the sample from the oven, **II** was treated with anhydrous benzene vapor to give the resultant material **III**.

Crystal Structures Determination. A. $\{[Zn_2(L)]\cdot 4H_2O\}_\infty$ (I). X-ray single-crystal diffraction data for **I** were collected at 150 K on a Bruker SMART APEX CCD area detector diffractometer using graphite-monochromated Mo Kα radiation. The colorless crystal was mounted on a dual stage glass fiber with silicon grease immediately on removal from the mother liquid. Crystal data for **I**: Tetragonal, $P4_22_12$, $a = b$ = 7.0249(7) Å, c =19.936(2) Å, V = 983.8(3) Å^3, T = 150 K, $C_{14}H_{12}N_2O_{12}Zn_2$, MW 531.04, Z = 2, D_{calcd} = 1.793 g/cm^3, μ = 2.504 mm^{-1}. Of 4888 reflections collected, 746 were independent with R_{int} = 0.027. The structure was solved by direct methods using SHELXS97[28] refined by least-squares on F^2 in SHEXLX97.[28] All non-hydrogen atoms were refined anisotropically, and framework hydrogen atoms were placed geometrically and refined as part of a riding model. Hydrogen atoms on the guest water molecules were not located from difference Fourier maps but were included in the formula. Final R_1 = 0.045 for 679 reflections with $I > 2\sigma(I)$, wR_2 = 0.124 for all 728 reflections, GOF = 1.095, $\Delta\rho_{max}$ = 0.85, $\Delta\rho_{min}$ = −0.40 Å^{-3}.

B. $[Zn_2(L)]_\infty$ (II). The crystal used in the above data collection for **I** was then mounted on a dual stage glass fiber using epoxy glue. The crystal was placed in a dry nitrogen gas flow at 293 K for 2 h, to remove the guest water molecules and convert compound **I** to **II**. Following this treatment of the crystal the diffraction pattern had altered and showed what appears to be a modulated structure with regular satellite reflections around peaks from the original lattice. Only the reflections fitting the original lattice were integrated and used for this study and were indexed as follows. Crystal data for **II**: Tetragonal, $P4_2/mnm$, $a = b$ = 7.0649(4) Å, c =19.775(2) Å, V = 987.03(13) Å^3, Z = 2, D_{calcd} = 1.544 g cm^{-3}, μ = 2.469 mm^{-1}. Of 5956 reflections collected, 752 were independent with R_{int} = 0.022. The structure was solved by direct methods using SHELXS97[28] refined by least-squares on F^2 in SHEXLX97.[28] All non-hydrogen atoms were refined anisotropically, and hydrogen atoms were placed geometrically and refined with a riding model. Diffuse electron density in the pore cavities was calculated and accounted for using SQUEEZE at 20 electrons per unit cell but the chemical species corresponding to this was not identified. Final R_1 = 0.059 for 291 reflections with $I > 2\sigma(I)$, wR_2 = 0.148 for all 505 reflections, GOF = 0.93, $\Delta\rho_{max}$ = 0.35, $\Delta\rho_{min}$ = −0.52 eÅ^{-3}.

In addition to single-crystal X-ray diffraction data for **I** and **II**, data were also collected for $[Zn_2(L)]_\infty$·0.55Benzene (**III**) at 150 K on a Bruker SMART APEX CCD area detector diffractometer using graphite-monochromated Mo Kα radiation. These data showed a similar pattern of satellite peaks around a tetragonal lattice which was indexed with the following unit cell parameters, $a = b$ = 7.0746(9) Å, c =19.774(2) Å, V = 989.7(4) Å^3. Although the data confirm that the framework structure remains intact, a fully satisfactory refinement could not be obtained in this case. Several other experiments attempting to study the removal of the guest water molecules *in situ* have also been carried out using a heated dry nitrogen gas flow and in one case using a room temperature helium gas flow, which in all cases show similar features around this basic tetragonal lattice. We are currently investigating these systems further in order to fully describe these modulated structures.

Gas and Vapor Adsorption Measurements. The nitrogen isotherms at 77 K were obtained by volumetric adsorption (Micrometrics ASAP 2020) and gravimetric (Hiden Isochema Intelligent Gravimetric Analyzer (IGA)) methods, yielding the same result. All other solvent vapors and gas isotherm measurements used the gravimetric (IGA) method. The crystalline sample of $\{[Zn_2(L)](H_2O)\}_\infty$ (**I**) was desolvated to generate $[Zn_2(L)]_\infty$ (**II**) by heating overnight at 423 K under a high vacuum (at least 10^{-6} mbar) until a constant mass was achieved. All isotherm data were corrected for buoyancy effects using the calculated density of **II** (1.545 g/cm^3) from the crystal structure determination of the framework only. The kinetic data were fitted by the IGASwin v1.03.143 [30] using a linear driving force model, and every isotherm datum was recorded only when >98.5% equilibration had been reached, with minimum and maximum logging times of 5 and 120 min, respectively. Each datum that timed out was fitted manually using the linear driving force model prior to any subsequent isotherm analysis.

Results and Discussion

Material Synthesis. The hydrothermal reaction of H_4L and excess $ZnCl_2$ in the temperature range of 110 °C to 150 °C in the presence of different bases all yielded the same compound, namely $\{[Zn_2(L)]\cdot 4H_2O\}_\infty$ (**I**). However, the additive base had a significant effect on product morphology (see photos provided in the Supporting Information). In the presence of NaOH, pyridine, triethylamine or di(isopropyl)amine, only microcrystalline products were separated, although powder XRD and elemental analysis have confirmed the consistency of their compositions. Two additives were found to be superior in promoting crystallinity in the product. In the presence of 2,6-lutidine/H_4L in a 4:1 ratio, microcrystalline product was isolated, but when the 2,6-lutidine/H_4L ratio was increased to 20:1, larger lath-shaped crystals (up to 0.3 mm in their longest dimension) were formed. Furthermore, cuboid crystals amenable to X-ray single-crystal diffraction were produced by the addition of a stoichiometric amount of 1,3,5-tri(4-pyridyl)-benzene (1,3,5-tpb/H_4L = 1.3:1). Products from the different preparative procedures were characterized by elemental analysis and IR spectroscopy which confirmed identical framework composition and by powder XRD confirming phase purity via comparison of experimental powder XRD patterns with those simulated from the single-crystal data.

Crystals of **I** exhibit much better stability than most known porous coordination framework compounds and are insoluble in water and in many common organic solvents. The coordina-

(28) Sheldrick, G. M. *SHELXL97* and *SHELXL97*. Programs for the Refinement of Crystal Structures. University of Göttingen (Germany): 1997.

(29) A.L. Spek. PLATON *J. Appl. Crystallogr.* **2003**, *36*, 7−13.

(30) IGASwin 1.03.143 Intelligent Gravimetric Analyzer Software, *Hiden Isochema Ltd:* Warrington, UK, **2005**.

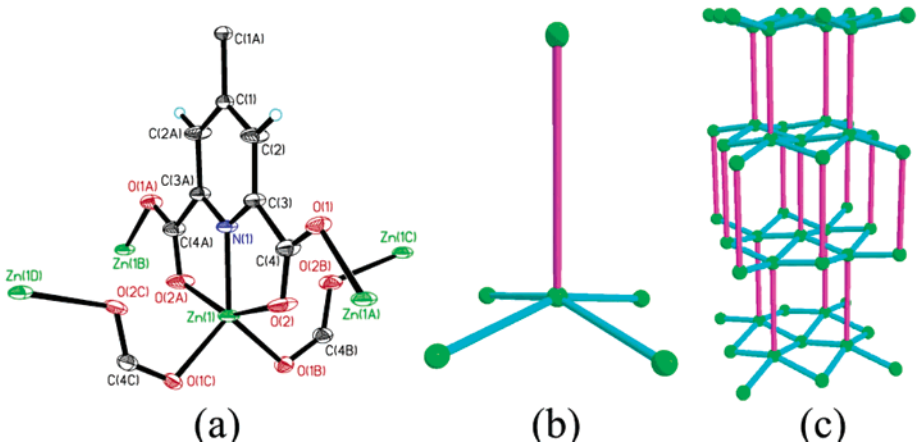

Figure 1. Crystal structure of $\{[Zn_2(L)]\cdot 4H_2O\}_\infty$ (**I**). (a) Coordination geometry of Zn(II); (b) a schematic view of the connections of one Zn(II) node; (c) the 4^46^6 topological network of **I**.

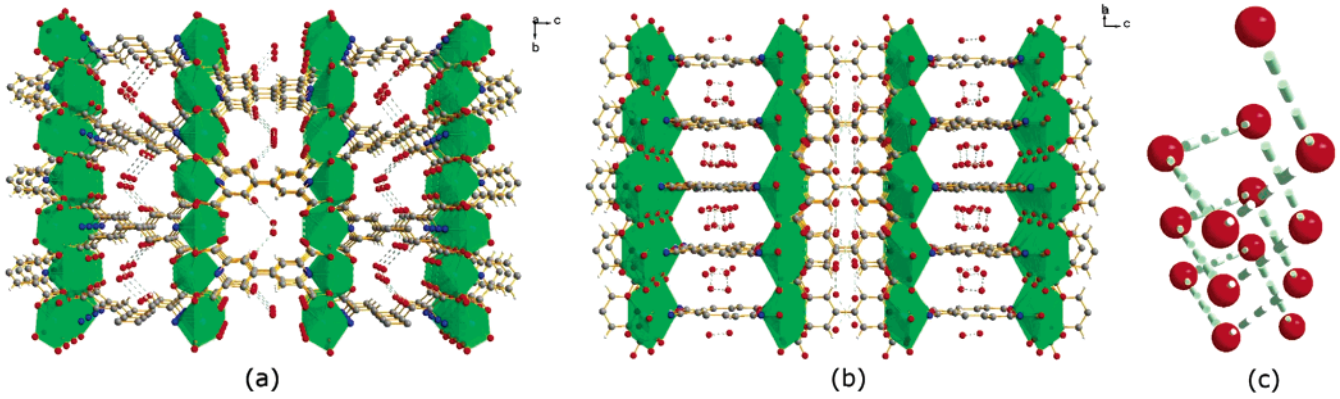

Figure 2. Framework structure of $\{[Zn_2(L)]\cdot 4H_2O\}_\infty$ (**I**), in which Zn(II) coordination spheres are represented by green polyhedron. (a) The view along the *a* axis shows the helical water molecule chains from the side; (b) the view along the *ab* diagonals; (c) the enlargement view of right-handed helical water chain.

tion geometry of $[Zn_2(L)]_\infty$ is also inert to substitution by other donor species such as pyridyl ligands, carboxylate, or $EDTA^{4-}$. The sample only decomposes in strong acid (e.g., aqueous HCl with pH $<$ 2) or in strong base (e.g., aqueous NaOH with pH $>$ 14).

Crystal Structure of I. The crystal structure of **I** shows a three-dimensional host framework with interconnecting pore cavities containing water molecules. The framework is constructed from Zn(II) ions and anionic ligands, L^{4-}. Zn(II) is coordinated by a tridentate array comprising two O-donors from 2,6-dicarboxylate groups and one pyridyl N-donor, all from the same ligand (Figure 1a). Two oxygen atoms, O(1B) and O(1C), from adjacent carboxylate groups bind to Zn(II) giving an O(1B)−Zn1−O(1C) bond angle of 99.13(19)° with the two coordination planes [O(1B)−Zn1−O(1C) and O(2)−Zn1−O(2A) in Figure 1a] perpendicular to each other by symmetry. The ligand sustains the 3-D framework through two different linkages (Figure 1c). The first one propagates along the pyridine−carboxylate chelating vector, i.e., the *c* axis of the unit cell via the N···N axis of the 4,4′-bipy molecule (schematically shown as purple sticks in Figure 1b); another is formed by the bridging carboxylate groups that propagate along the *ab* face diagonals (blue sticks in Figure 1b). The bridging links result in the formation of a rare five-connected structure[31] with 4^46^6 topology. X-ray structure analysis reveals the helical chains of water molecules within the channel along the *ab* face diagonals (Figure 2). Although the positions of the water hydrogen atoms could not be located, the O···O separation of 2.852(12) Å and 2.909(14) Å suggests the presence of hydrogen-bonding between neighboring water molecules.

I crystallizes in the chiral space group $P4_22_12$, and even more interestingly the framework of **I** itself is nonchiral. The chirality of the crystal is thus generated by the guest entities comprising helical water molecule chains. PLATON[29] calculates that 88% of the atomic sites in **I** fit the higher symmetry space group $P4_2/mnm$, but refinement in this space group, involving a disordered water model, is very poor. The refinement in $P4_22_12$ approximately halves the uncertainty (s.u. on Zn−O bond falls from 0.006 to 0.003 Å) and reduces the *R*-factor wR_2 from 20.3% to 12.4% compared to refinement in $P4_2/mnm$. The Flack parameter 0.56(9) indicates that the crystal of **I** is a racemic twin and that there are both left-handed and right-handed helical water molecular chains present in this sample of **I**. Figure 2c shows a right-handed helical water molecular chain within the crystal structure of **I**.

It is noteworthy that the guest water molecules in **I** are bound inside the channel with very weak C−H···O hydrogen-bonding between water molecules and C−H moieties of the pyridine-rings. There appear to be no strong O−H···O hydrogen bonding contacts between the guest water molecules and the host

(31) Long, D.-L.; Blake, A. J.; Champness, N. R.; Wilson, C.; Schröder, M. *J. Am. Chem. Soc.* **2001**, *123*, 3401−3402. (b) Hill, R. J.; Long, D.-L.; Turvey, M. S.; Blake, A. J.; Champness, N. R.; Hubberstey, P.; Wilson, C.; Schröder, M. *Chem. Comm.* **2004**, 1792−1793. Hill, R. J.; Long, D.-L.; Champness, N. R.; Hubberstey, P.; Schröder, M. *Acc. Chem. Res.* **2005**, *38*, 335−348.

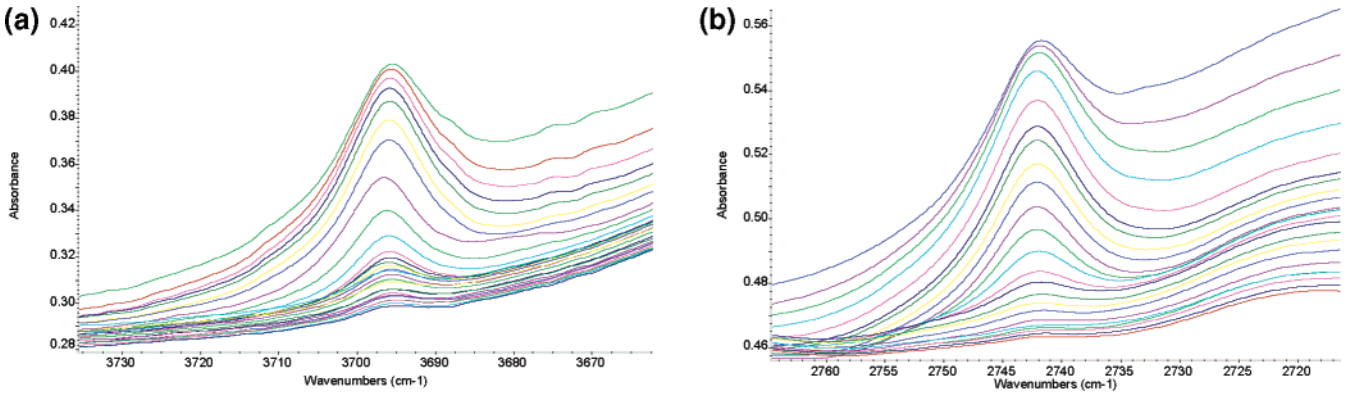

Figure 3. Diffuse reflectance IR spectra (DRIFTS) of complex **I**: (a) H_2O peak at 3696 cm^{-1} reduced to very low intensity when exposed to a dry N_2 atmosphere; and (b) the comparison experiment with D_2O shows the same removal process of D_2O, but the peak is at 2742 cm^{-1}.

framework. This observation provides an explanation for the ease of removal of water molecules from the lattice, resulting in the compound **II** which has a window of 3.9 Å × 5.1 Å and interconnecting cavities, which are accessible by other small molecules (see below). The void volume in **II** is calculated by PLATON[29] to be 32.6% of the total volume.

Crystal Structure of II. Crystals of **II** were prepared by dehydrating a crystal of **I** by placing the crystal in a dry nitrogen gas flow at 293 K for 2 h (see below for a discussion of the dehydration process for **I**/**II**). The single-crystal data for **II** reveals a significantly different appearance from that observed for **I**. In particular regular satellite reflections around peaks from the original lattice indicated the formation of a modulated structure. However, a structural solution could be obtained for **II** confirming retention of the framework structure with highly similar structural parameters to those observed for **I**. Analysis of the framework pores using the SQUEEZE procedure within the PLATON suite[29] indicated the presence of residual diffuse electron density in the pore cavities, but this could not be chemically identified (ca. 20 electrons per unit cell, potentially corresponding to 2 H_2O molecules per unit cell in comparison to 8 H_2O molecules per unit cell in the structure of **I**). It is clear that the water molecules no longer sit in defined positions within the framework structure, but that diffuse electron density, potentially representing water molecules, remains within the pores. This is unsurprising when taking into account the adsorption/desorption behavior of **I**/**II** as discussed below.

Framework Stability and Gas Adsorption and Desorption. The water molecules accommodated within framework **I** can be monitored by DRIFTS FTIR spectroscopy. The spectra were recorded over a period of 3 h while purging the sample chamber with N_2 gas. Figure 3a shows the variation of the adsorption at 3696 cm^{-1}, assigned to the stretching vibration of adsorbed water molecules in the channels and is clearly not due to bulk water.[32] This sample was then exposed to a D_2O vapor for a period of 30 min before remeasurement of the spectra resulting in the observation of the corresponding D_2O stretching vibration at 2742 cm^{-1}. As in the case of adsorbed H_2O, the intensity of this D_2O-based peak was reduced in intensity by purging the chamber with N_2 until it was almost entirely removed(Figure 3b), indicating that water molecules in the framework can be removed simply by exposure of the sample under a dry environment without heating.

(32) Pimentel, G. C.; McClellan, A. L. *The Hydrogen Bond*; W. H. Freeman, San Francisco, CA, 1960.

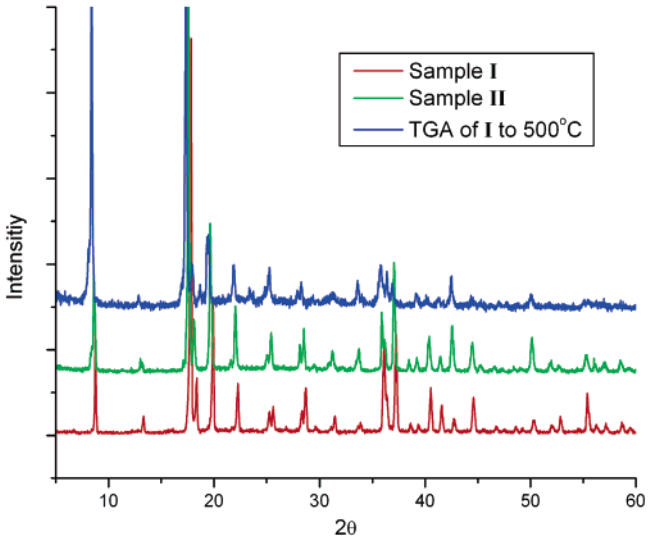

Figure 4. Powder XRD patterns of **I**, **II** and a sample of **I** after TGA to 500 °C.

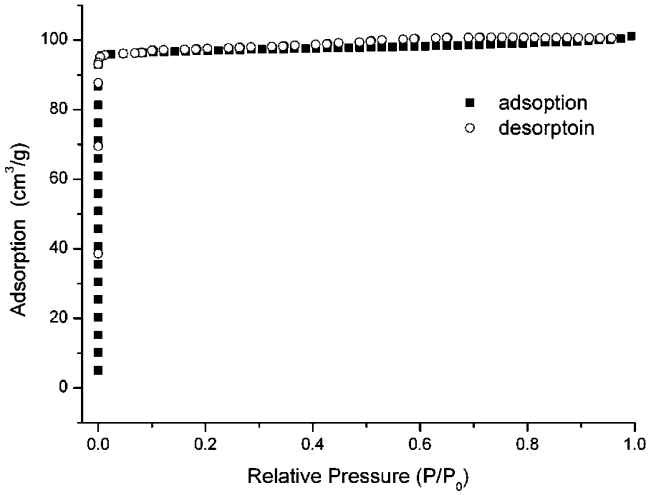

Figure 5. Adsorption-desorption isotherm of **II** at 77 K obtained with N_2 gas in the relative pressure range from 10^{-6} to 1 atm at 77 K.

The studies of thermal stability and gas absorption properties of compound **I** have been carried out by combining TGA, powder XRD, and gas isotherm measurements. The microcrystalline sample **I** loses water very rapidly as anticipated from the DRIFTS experiments. At 70 °C, the total weight loss is about 12.8%, slightly lower than the calculated water content (13.5%)

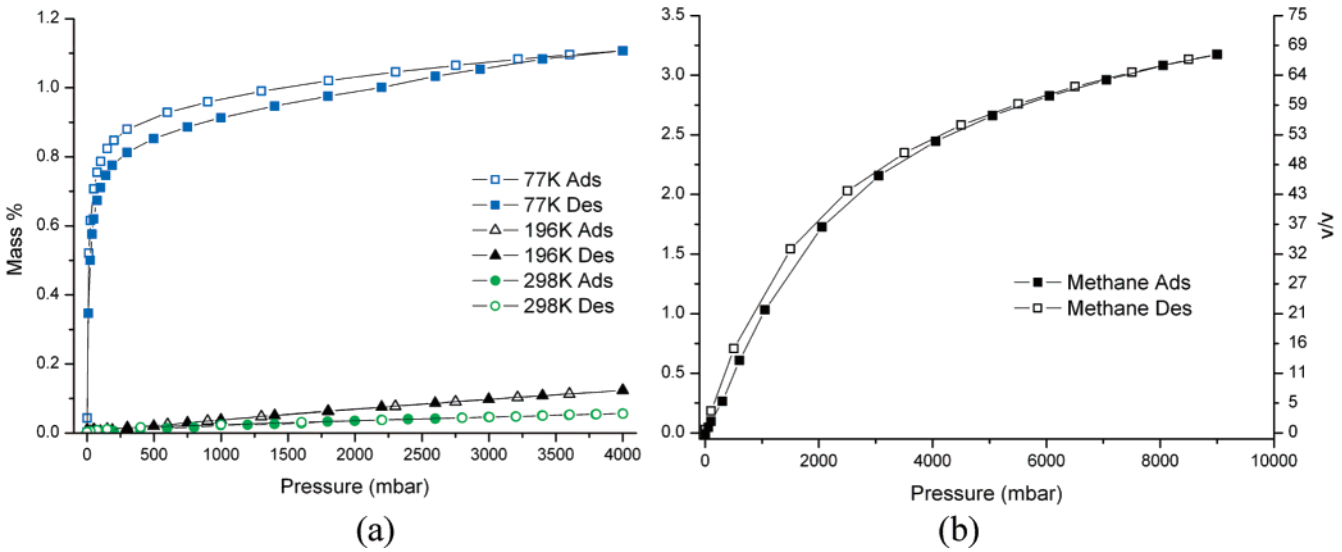

Figure 6. Adsorption and desorption isotherm of **II** obtained with (a) H_2 gas at three different temperatures (77, 196, and 298 K) and (b) CH_4 gas at 298 K.

obtained from X-ray single-crystal structure analysis. This difference is attributed to the sample used for the TGA experiment losing some water after removal from water solution and prior to the TGA experiment.

The framework of compound **I** has a high thermal stability. According to the TGA and DSC data, no phase change was recorded after the removal of the water molecules from the channels up to 250 °C in air or 450 °C under a nitrogen atmosphere, above which the framework starts to decompose. By microscopy and powder XRD, a sample can be heated to 150 °C in air for 4 months without losing crystallinity, although it slowly decomposes above 200 °C. Under N_2, however, the material is stable up to 450 °C. Figure 4 confirms that considerable crystallinity remains, even after the sample has been heated to 500 °C in a TGA experiment, with only small levels of peak broadening observed.

The excellent framework stability of **II** provides an opportunity to probe gas adsorption properties. The isotherm obtained with N_2 gas at 78 K revealed a typical Type-I adsorption curve as defined by the IUPAC classification scheme[33] (Figure 5). The nitrogen adsorption increases abruptly at the start of the experiment and reaches a plateau of 97 cm^3 (STP)/g at $P/P_0 = 0.05$, indicating a uniform structured micropore corresponding to 4.1 N_2 molecules in each unit cell. The adsorption isotherm data were fitted to the BET equation to give a BET surface area of 312.7 m^2/g and to the Langmuir equation giving a surface area of 423.7 m^2/g. Using the t-plot model, the pore volume is 0.146 cm^3/g, which is smaller than the pore volume of 0.187 cm^3/g calculated from the crystal structure: this discrepancy can be attributed to the N_2 molecules being unable to fill the void space efficiently. Using the Horvath−Kawazoe (HK) method, a very narrow pore width distribution centered at 5.2 Å was obtained, which is consistent with the single-crystal structure analysis.

The framework **II** reversibly adsorbs and desorbs H_2 at 77 K, and typical Type-I adsorption behavior was observed (Figure 6). The H_2 adsorption data can be fitted by the linear

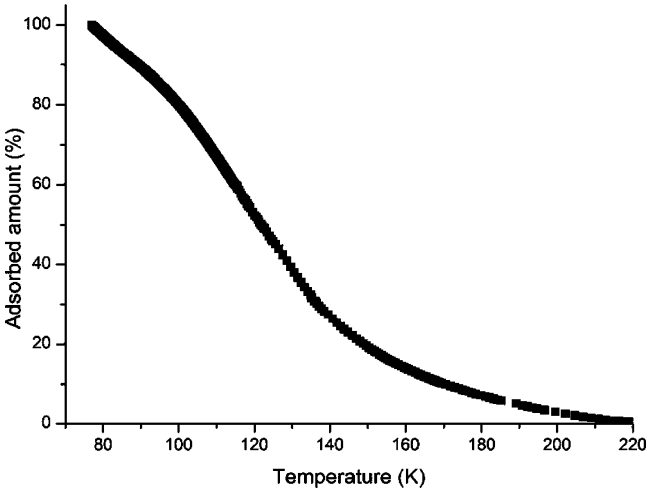

Figure 7. H_2 Isobar of **II**.

Langmuir equation, predicting a maximum uptake of 1.08 wt %, which was experimentally observed at 4 bar. The observed H_2 adsorption at 300mbar is 0.8 wt %, and almost reaches a plateau indicative of strong micropore filling relative to most known coordination frameworks which adsorb hydrogen.[13,16,17,23] By using a value for the density of liquid hydrogen of 0.077 g/cm^3 at the triple point (14 K), the volume of H_2 adsorbed on **II** is 0.158 cm^3/g, corresponding to 21.3% occupancy and 4.9 hydrogen molecules in each unit cell.

It is noteworthy that this occupancy is even higher than that of N_2 saturated **II** at 77 K (17.7%) and may be due to the fact that the smaller H_2 molecules can fill the pores more efficiently. At 195 K and 298 K, **II** can adsorb only very small amounts of H_2 (0.12 wt % and 0.057 wt % at 4 bar, respectively) and shows a linear uptake relationship (known as "Henry's Law"). Henry's Law is predicted to be observed in the very low-coverage region, where interaction between adsorbed molecules may be neglected and the only remaining interactions are those between single molecules and the surface.[34]

Methane adsorption at 298 K corresponds to 3.14 wt % (44.0 cm^3/g or 67 v/v) at 9 bar (Figure 6) and 14.1% occupancy of the unit cell. Although this adsorption is low relative to the

(33) Rouquerol, F.; Rouquerol, J.; Sing, K. *Adsorption by Powders and Porous Solids*; Academic Press: London, 1999.

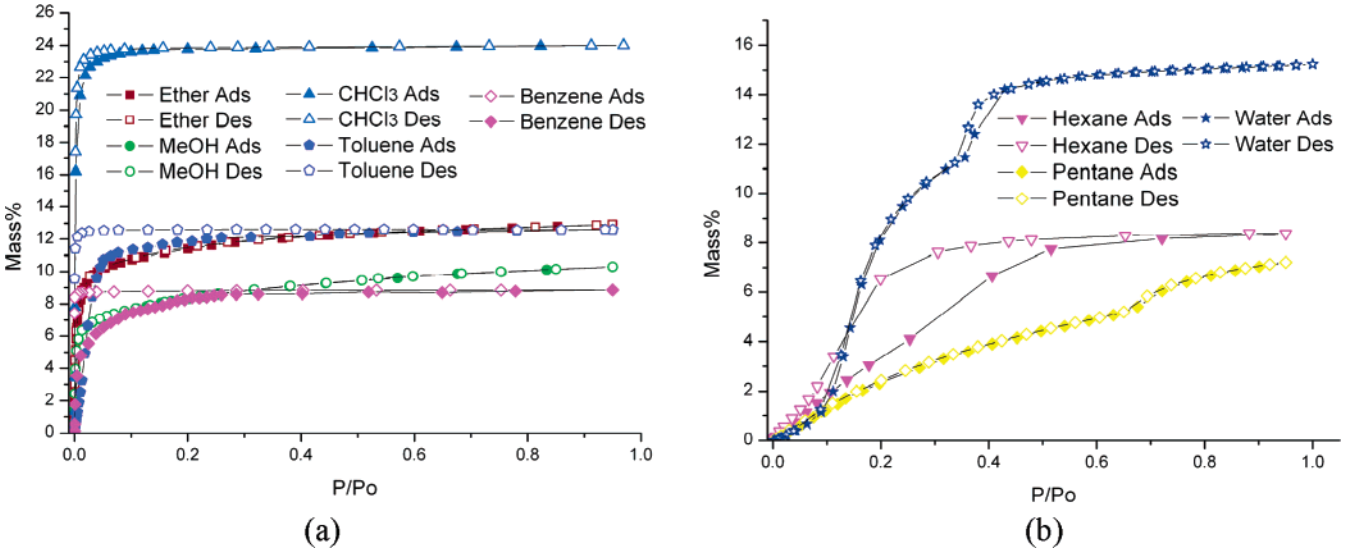

Figure 8. Adsorption and desorption isotherms of different solvent vapors on **II** at 298 K.

filling level of other guest species, the adsorption curve lies close to the saturation plateau (Figure 6), and therefore little further uptake can be expected. The estimated maximum amount of CH_4 adsorption on **II**, obtained by fitting of CH_4 adsorption data to the Langmuir plot, is 4.27 wt % (59.8 cm^3/g or 91 v/v).

Figure 7 shows the isobar for H_2 adsorption at 1 bar. H_2 adsorption on **II** is very sensitive to temperature, and the adsorption decreases rapidly with increasing temperature. Very slight curvature is observed below 110 K, and this behavior is comparable with that observed on activated carbon which has a microporous structure.[15] However, **II** does not show the capability to trap H_2 molecules at low temperature, which was observed for $Ni_2(bipy)_3(NO_3)_4$,[15] suggesting that a more flexible framework may be more promising in H_2 storage than the rigid framework of **II**, activated carbon, or zeolites.

The permanent porosity of **II** allows access by a variety of small molecules, and the different affinities between guest molecules and the host framework affect the mobility and volatility of solvent molecules within the framework. The solvent vapor adsorption isotherms on **II** can be classified according to the interaction strength of guest molecules and host framework. Chloroform, methanol, ether, benzene, and toluene have a typical Type-I isotherm (Figure 8a). In the low P/P_0 region, the adsorptions of these vapors reached saturation indicating a strong guest−host interaction. In contrast, the adsorption of hexane, pentane, and water shows weak interaction with the framework as supported by the observation that the amount of adsorption increases gradually along with the increasing relative pressure of absorbates (Figure 8b).

The strength of interaction of guest molecules and host framework can depend on several factors. It is possible that supramolecular interactions between the guest species and the framework account for the different types of adsorption processes. Thus, MeOH and $CHCl_3$ are both capable of hydrogen-bonding interactions with the host framework, and toluene and benzene are likely to participate in $\pi-\pi$ interactions with the ligands in the framework. Accordingly, pentane and hexane are both relatively inert in a supramolecular sense, presenting no hydrogen-bonding or $\pi-\pi$ interaction capability, leading to a slow uptake of these two species.

However, two unusual features appear in the data. First, diethyl ether is a poor hydrogen-bond acceptor and thus would be expected to behave in a manner similar to pentane and hexane, whereas it experiences rapid uptake by the framework. Perhaps more surprising is the behavior of water which is clearly capable of hydrogen-bonding to the framework structure. However, the crystal structure of **I**, coupled with the DRIFTS measurements, indicates that the H_2O molecules more readily hydrogen-bond to other H_2O molecules rather than to the framework. The observation of H_2O-H_2O interactions as opposed to H_2O−framework interactions may account for the seemingly anomalous and to us surprising adsorption behavior of water, rendering water inert (in a supramolecular sense) in terms of absorbate−absorbent interactions. In conclusion, it should be noted that the precise nature of interactions between the framework and the absorbates is purely speculative and in the absence of crystal structures remains difficult to evaluate with precision.

The isotherms were studied using the Dubinin−Radushkevich (DR) equation to characterize the porosity of **II**. Because both H_2 and CH_4 are supercritical under the experimental conditions, the DR equation (1) was used to analyze hydrogen and methane isotherms.

$$RT \ln P = RT \ln P_{0q} - \beta E_0 \sqrt{\ln\left(\frac{W_0}{W}\right)} \qquad (1)$$

where W_0 is the estimated maximum uptake obtained from the Langmuir plot, P_{0q} is the saturated vapor pressure of the quasi-vaporized supercritical gas, and βE_0 is the adsorption energy. The adsorption energy βE_0 is the slope of the plot.

For nitrogen and solvent vapors, a variant of DR equation (2) was used in the analysis. In the high relative pressure (P/P_0) region, the DR plot has a linear relationship which wasused to deduce the value of βE_0.

$$\ln W = \ln W_0 - \left(\frac{RT}{\beta E_0}\right)^2 \left(\ln\left(\frac{P_0}{P}\right)\right)^2 \qquad (2)$$

(34) Dash, J. G. *Films on solid surfaces: The Physics and Chemistry of Physical Adsorption*; Academic Press: London, 1975.

Table 1. Micropore Parameters of Compound **II** by Different Absorbates from DR Analysis

	calcd	N_2	H_2	CH_4	H_2O	benzene	$CHCl_3$	MeOH	hexane	pentane	Et_2O	toluene
Vocc[a] (%)	32.6[f]	17.7	21.3[c]	14.1[c]	22.8	15.4	22.3	20.1	19.1	17.5	26.0	21.9
no. mole[b]	n/a	4.10	4.90[c]	2.49[c]	7.65	1.06	1.84	2.95	0.91	0.92	1.49	1.25
W_0 (cc/g)	n/a	97.2	1.08[d]	59.8	192	25.7	45.0	58.4	13.6	12.7	36.5	30.3
βE_0 (kJ mol^{-1})	n/a	29.6	4.20	8.38	5.03	13.4	42.0	19.6	6.39	5.82	18.2	18.3
$q_{st,\Phi=1/e}$ (kJ mol^{-1})	n/a	35.2	5.12[e]	16.54[e]	45.7	47.3	73.4	57.4	38.1	32.56	45.6	56.4

[a] Volume occupancy percentage in the unit cell. [b] Number of adsorbed molecules in each unit cell. [c] Estimated value from Langmuir plot. [d] Mass percentage. [e] The ΔH_v of gases at their bp was used (H_2 = 0.92 kJ mol^{-1} at 20 K, CH_4 = 8.16 kJ mol^{-1} at 111 K).[35] [f] Calculated from the crystal structure of **I** using PLATON.[29]

W_0 in equation (2) is the maximum uptake obtained from experiments at the saturated vapor pressure P_0.

Table 1 lists the volume occupancies of different guest species in the framework of **II** from the uptakes recorded at the maximum gas or vapor pressure. The condensation of solvent vapors inside the framework is determined by two energies, the adsorption energy βE_0 and the vaporization heat ΔH_v of solvents. Thus, the isosteric heat of adsorption, $q_{st,\Phi=1/e}$, at the fractional filling of $1/e$ can be obtained by using $q_{st,\Phi=1/e} = \Delta H_v + \beta E_0$, where ΔH_v is the heat of vaporization of solvents. Therefore, we can quantify the strength of interaction between the guest species and host framework. The adsorption energy βE_0, which indicates the interaction strength of guest molecules and the host framework, dominates the initial adsorption process in the low P/P_0 region. The larger adsorption energy βE_0 drives the adsorption, reaching saturation quickly at low P/P_0. Along with the increase of P/P_0, the condensation of solvent vapors dominates the adsorption process. Therefore, the adsorption of pentane vapor only reaches its maximum near P_0, while hexane reaches saturation at $P/P_0 = 0.6$ due to its higher heat of vaporization.

The isosteric heat is a measure of the strength of the interaction between adsorbent and adsorbate. Complex **II** shows a remarkable affinity to N_2 with an isosteric heat $q_{st,\Phi=1/e}$ at 77 K of 35.2 kJ mol^{-1}, much larger than that on active carbon[36] (~12 kJ mol^{-1}) or on other metal−organic framework compounds (13.0 kJ mol^{-1} for $[Cu_2(pzdc)_2(bpy)]_\infty$,[37] 15.7 kJ mol^{-1} for $\{[Cu_2(4,4'\text{-bpy})(PF_6)(NO_3)](PF_6)_2 \cdot 2(H_2O)\}_\infty$,[9] and 7.68 kJ mol^{-1} for $[Ni_3(btc)_2(3\text{-pic})_6(1,2\text{-pd})_3]_\infty$[12]). However, the isosteric heat of H_2 on **II** at 77 K is only 5.12 kJ mol^{-1}, which is only slightly higher than that on active carbon[15] (~4 kJ mol^{-1}). For hydrogen storage, due to the very small ΔH_v of H_2 (0.92 kJ mol^{-1}), the value of adsorption energy βE_0 determines the adsorption behavior. Therefore, with a small difference between 5.12 kJ mol^{-1} for **II** and 4 kJ mol^{-1} for carbon, the amount of adsorbed H_2 in **II** can rapidly approach its maximum capacity at low pressure (0.3 bar). This represents a potential methodology for preparing materials for physio-sorption of H_2 at lower pressure and higher temperature. Unfortunately, the small pore volume of **II** prevents higher adsorption capacities. For CH_4 gas, the isosteric heat of 16.54 kJ mol^{-1} of CH_4 on **II** at 298 K suggests that its affinity for CH_4 molecules is similar to that of activated carbon fibers (17−18 kJ mol^{-1})[38] and other metal−organic framework compounds (16.3 kJ mol^{-1} for $[Cd(NO_3)_4(azpy)_3]_\infty$, 20.2 kJ mol^{-1} for $[Co(NCS)_2(azpy)_2]_\infty$,[39] and 9.0−15.5 kJ mol^{-1} for a range of framework compounds[18]). Therefore, we can conclude that **II** has selectivity for N_2. The mechanism of this selectivity in comparison to other coordination framework or active carbon materials is still unknown but must be related to a particular shape or feature of the porous structure.

The weak binding of water molecules to the framework is an interesting phenomenon. Water has very low adsorption energy, $\beta E_0 = 5.03$ kJ mol^{-1}, indicating that the host framework provides a hydrophobic environment. Therefore, in the low P/P_0 region, water molecules are hardly adsorbed. However, the high heat of vaporization of water dominates the adsorption behavior in the higher P/P_0 region (>0.1); i.e., the intermolecular water−water interactions promote the condensation of water molecules inside the pores. The isotherm of water has a stepwise behavior, and a hysteretic loop is observed at $P/P_0 = 0.4$. Similar behavior has also been observed in the nitrogen isotherm of some microporous zeolites.[40] This has been explained by a fluid-to-crystalline-like phase transition of the adsorbed phase within the micropores and does not indicate any real porosity. Considering the very sharp pore distribution obtained from the N_2 isotherm and the high crystallinity characterized by power XRD, no other porosity can be attributed to the second step adsorption in the water isotherm. Therefore, we believe that this fluid-to-crystalline-like phase transition occurs on adsorption of water molecules in the framework. This is also supported by the isotherm data of water vapor at different temperatures (Figure 9). At low temperature, this phase transition occurs at low relative pressure and has a significant second uptake, which becomes less noticeable with increasing temperature. Similarly, we noticed that pentane also shows a slight stepwise adsorption behavior, which may also relate to a phase transition phenomenon.

The adsorption/desorption kinetics of guest molecules in the framework are related to the guest−host interaction. A kinetic trap effect was observed for large absorbate substrates (benzene, toluene, and hexane) within the framework **II**. We found that benzene has the most significant effect, and benzene molecules can only be completely removed at the end of the desorption scan under a high vacuum ($<10^{-3}$ mbar) when heated up to 70 °C. The flat benzene molecule has potentially the strongest $\pi-\pi$ interaction with the framework, and toluene is more easily removed under vacuum, presumably due to the methyl group

(35) Vaporization heat of hydrogen and methane obtained from: http://www.airliquide.com/en/business/products/gases/gasdata/index.asp.
(36) (a) Kaneko, K.; Shimizu, K.; Suzuki, T. *J. Chem. Phys.* **1992**, *97*, 8705−8711. (b) Dubinin, M. M. *Carbon* **1987**, *25*, 593−598.
(37) Matsuda, R.; Kitaura, R.; Kitagawa, S.; Kubota, Y.; Kobayashi, T. C.; Horike, S.; Takata, M. *J. Am. Chem. Soc*. **2004**, *126*, 14063−14070.
(38) Kaneko, K.; Murata, K.; Shimizu, K.; Camara, S.; Suzuki, T. *Langmuir* **1993**, *9*, 1165−1167.
(39) Kondo, M.; Shimamura, M.; Noro, S.; Minakoshi, S.; Asami, A.; Seki, K.; Kitagawa, S. *Chem. Mater*. **2000**, *12*, 1288−1299.
(40) (a) Bonardet, J.; Fraissard, J.; Unger, K.; Kumar, D.; Ferrero, M.; Ragle, J.; Conner, W. C. The Use Of N^{15} NMR For The Understanding Of Nitrogen Physisorption. In *Characterization Of Porous Solids − III*, Elsevier Science B. V.: Amsterdam, 1994; Vol. 87, pp 319−326. (b) Groen, J. C.; Peffer, L. A. A.; Perez-Ramirez, J. *Microporous Mesoporous Mater*. **2003**, *60*, 1−17.

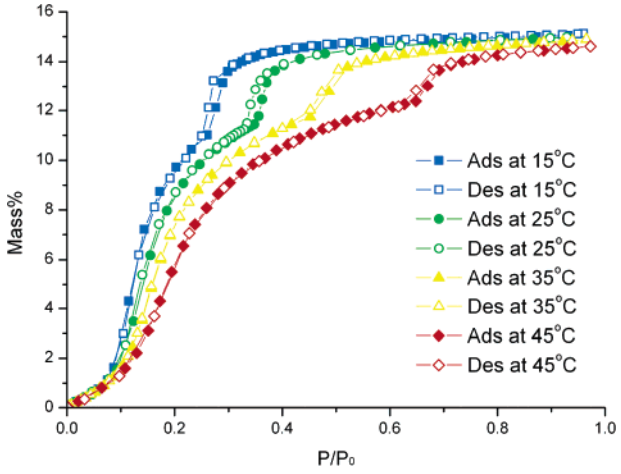

Figure 9. Isotherms of water vapor on **II** at different temperatures.

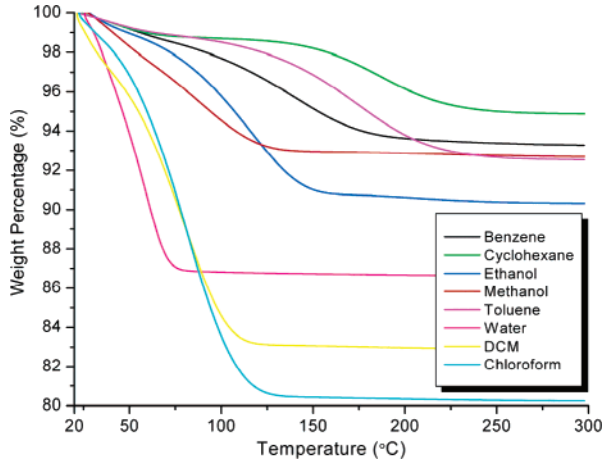

Figure 10. TGA of **II** with different absorbates.

of the toluene molecule inhibiting this $\pi-\pi$ interaction. Hexane also has a significant adsorption−desorption hysteretic loop, but adsorbed hexane can be removed under vacuum more readily due its low isosteric heat.

The kinetic trap effects were monitored by TGA. At a scan rate of 2 °C/min and under a N_2 flow of 100 mL/min, the TGA curves of samples of **II** loaded with substrates showed inflection points for most solvents that were higher than their boiling points (Figure 10). The increase of the inflection points of large molecules is much greater than those for small molecules. As shown in Figure 10, benzene, cyclohexane, and toluene were not completely removed until the temperature exceeded 200 °C, which is more than 100 °C higher than their boiling points. For other small solvent molecules such as CH_2Cl_2, $CHCl_3$, methanol, and ethanol, this difference is about 70 °C. This indicates that the framework structure limits the motion and diffusion of larger molecules more significantly than of smaller molecules. The TGA behaviors of CH_2Cl_2 and $CHCl_3$ in **II** are very similar. However, CCl_4 cannot be adsorbed by **II** due to the smallest dimension of the CCl_4 molecule (5.723 Å[41]) molecule exceeding the size of the channels of **II**. Thus, CCl_4 cannot access the voids in **II**, and any slight structural breathing which may take place for flat molecules, such as toluene or benzene, does not allow the inclusion of CCl_4. Compared to organic solvents, the behavior of water is an exception in that the inflection at 70 °C is much lower than the boiling point of water suggesting that the OH···O hydrogen-bonding in liquid water, has been limited by the hydrophobic framework, and the trapped water molecules show greater volatility than organic solvent molecules.

Summary

This contribution has described the synthesis and properties of a coordination framework $\{[Zn_2(L)]\cdot 4H_2O\}_\infty$ (**I**), prepared by hydrothermal reaction of $ZnCl_2$ and 4,4′-bipyridine-2,6,2′,6′-tetracarboxylic acid (H_4L). The structure of **I** confirms it to be an unusual 5-connected network with a 4^46^6 topology comprising Zn(II) bound to L^{4-}. The water molecules in the as-synthesized material can be readily removed by heating the sample in a vacuum to yield $[Zn_2(L)]_\infty$ (**II**), and this resulting porous material has a very high thermal stability and is highly robust and chemically inert. A 1.08 wt % hydrogen uptake was observed for this material at 4 bar. The isotherms of various solvent substrates in **II** have allowed us to probe the different interactions between guest species and pore walls, which are dominated by different supramolecular interactions. Further DR analysis of the isotherm data revealed two different adsorption behaviors driven by absorbate−absorbate or absorbate−absorbent interactions. High absorbate−absorbent interaction energy results in the adsorption reaching saturation at low relative pressure, while absorbate−absorbate interactions act only in the high relative pressure region, promoting the condensation of absorbate inside the framework. DR analysis also suggests that the framework **II** has a high affinity for N_2 relative to other microporous materials and a slightly higher affinity for hydrogen molecules compared to other coordination framework compounds.

Acknowledgment. This work was supported by the EPSRC Supergen (UKSHEC) Initiative. M.S. acknowledges receipt of a Royal Society Wolfson Merit Award and of a Leverhulme Trust Senior Research Fellowship. We also thank Professor J. A. K. Howard (University of Durham) for crystallographic studies.

Supporting Information Available: Additional views of the crystal structure, pictures, TGA data, powder XRD data, Langmuir plots and DR plots, and X-ray crystallographic files (CIF). This material is available free of charge via the Internet at http://pubs.acs.org.

JA060946U

(41) Webster, C. E.; Drago, R. S.; Zerner, M. C. *J. Am. Chem. Soc.* **1998**, *120*, 5509−5516.